



Insights into Protein Dynamics from ^{15}N - ^1H HSQC

Erik R.P. Zuiderweg

Department of Biological Chemistry, The University of Michigan, Ann Arbor, MI48109, USA
and

5 Institute for Molecules and Materials, Faculty of Science, Radboud University Nijmegen, 6525 XZ,
The Netherlands.

Correspondence to: Erik R.P. Zuiderweg (zuiderwe@umich.edu)

Abstract. Protein dynamic information is customarily extracted from ^{15}N NMR spin-relaxation experiments. These experiments can only be applied to (small) proteins that can be dissolved to high concentrations. However, most proteins of interest to the biochemical and biomedical community are large and relatively insoluble. These proteins often have functional conformational changes, and it is particularly regretful that these processes cannot be supplemented by dynamical information from NMR. We ask here whether (some) dynamic information can be obtained from the ^1H line widths in ^{15}N - ^1H HSQC spectra. Such spectra are widely available, also for larger proteins. We developed computer programs to predict amide proton line widths from (crystal) structures. We aim to answer the following basic questions: is the ^1H linewidth of a HSQC cross peak smaller than average because its ^1H nucleus has few dipolar neighbors, or because the resonance is motionally narrowed? Is a broad line broad because of conformational exchange, or because the ^1H nucleus resides in a dense proton environment? We calibrate our programs by comparing computational and experimental results for GB1 (58 residues). We deduce that GB1 has low average ^1HN order parameters (0.8), in broad agreement with what was found by others from ^{15}N relaxation experiments (Idiyatullin et al., 2003). We apply the program to the BPTI crystal structure and compare the results with a ^{15}N - ^1H HSQC spectrum of BPTI (56 residues) and identify a cluster of conformationally broadened ^1HN resonances that belong to an area, for which millisecond dynamics has been previously reported from ^{15}N relaxation data (Szyperski et al., J. Biomol. NMR 3, 151-164, 1993). We feel that our computational approach is useful to glean insights into the dynamical properties of larger biomolecules for which high-quality ^{15}N relaxation data cannot be recorded.

25

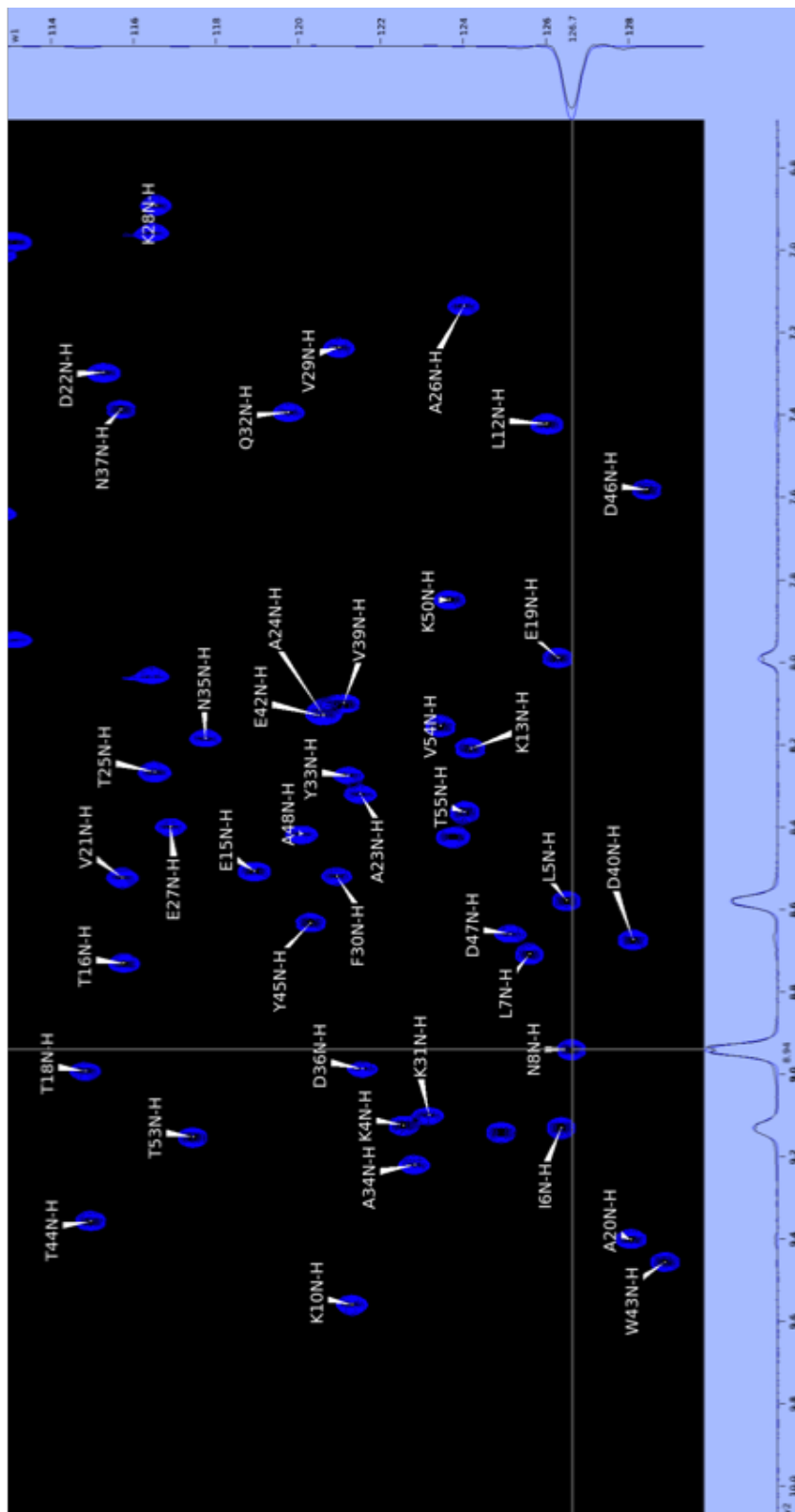


1. Introduction

Providing evidence that proteins are dynamical rather than rigid molecules is a major contribution of solution NMR to structural biology and molecular biophysics (Kay, 1998). The dynamic information is extracted from NMR spin-relaxation experiments, mostly of the amide nitrogen (Kay et al., 1989), but also from methyls (Nicholson et al., 1992) (Lee et al., 2000) and from carbonyl (Wang et al., 2006). The amide nitrogen relaxation experiments are the easiest to implement, require just ^{15}N isotopic labeling, are potentially complete, and analysis software is broadly available (Mandel et al., 1995). But these experiments are rather insensitive (especially the $^1\text{H} \rightarrow ^{15}\text{N}$ NOE) and can therefore only be applied to (small) proteins that can be dissolved to high concentrations.

However, most proteins of interest to the biochemical and biomedical community are large, and cannot be studied with ^{15}N dynamics measurements. This is particularly regretful, because larger proteins, more than smaller, often display functional conformational changes which cannot be supplemented by dynamical information from NMR. Moreover, considering the insight that fast dynamics contributes to configurational entropy (Akke et al., 1993) (Yang and Kay, 1996) (Lee et al., 2000), lack of measurement of dynamics also results in the lack of (experimental) understanding of the protein's thermodynamics. Due to the paucity of dynamical measurements of the proteins of interest to the biochemical and biomedical community, the above "dynamics awareness" has not generally taken hold in that important area of science and medicine, which I find regretful. However, ^{15}N - ^1H HSQC and TROSY HSQC experiments can be recorded for (very) large proteins (< 300 kDa) at relatively low concentrations (< 50 μM). This experiment contains conformational dynamics information in the intensity and line widths of its cross peaks. In this contribution, we explore if we can harvest (some) of the dynamical information from that data, without the need for specific "relaxation" experiments and/or labeling strategies (Gardner et al., 1997).

The study of a protein by solution NMR usually starts by recording such a ^1HN - ^{15}N HSQC or TROSY HSQC spectrum of the sample. Such a dataset is seen as a "fingerprint" of the protein, from which important molecular parameters can immediately be gleaned. For instance, an experienced NMR spectroscopist recognizes from such a spectrum whether the sample is pure, the protein is (mostly) folded, whether it aggregates, or whether it has multiple conformations. Looking into more detail, the spectroscopist finds that the ^1HN linewidths of the cross peaks will differ from each other (not when a dominating windowing function was used). The spectroscopist may want to infer that lines narrower than average are due to fast dynamics, and broad lines to conformational exchange processes. But such inferences are not warranted. Amide proton linewidths may be affected by a plethora of mechanisms, which we will try to unravel in this work. Only after that we can answer the question: is a narrow line narrow because it has few dipolar neighbors, or is it motionally narrowed? Is a broad line broad because of conformational exchange, or because it has a dense proton environment?





60

Figure 1. Section of the 600 MHz ^{15}N - ^1H HSQC spectrum of GB1 at 3 °C, pH 6.5. Processed with 1 Hz EM in t_2 , \cos^2 in t_1 . The assignments were taken from BMRB entries 7280, 25909 and 26716. The numbering is as in PDB entry 6c9o.pdb. The cross sections show the Gaussian line shape fits as carried out by Sparky (Goddard and Kneller, 2000)

Let us take a look at the ^{15}N - ^1H HSQC spectrum of GB1 (Figure 1). We take this protein as our “calibration” case. The assignments are available at the Biological Magnetic Resonance Bank, while high-resolution crystal structures are available in the Protein Data Bank. The intensities of the cross peaks in the spectrum vary by a factor of 3 and the ^1HN linewidths vary by a factor 2 (see Table S1 in the Supplemental Materials). The spectrum shows several doublets (e.g. N8), due to the 3JHNHA coupling. What causes the variation in ^1HN line width? There are several possibilities. First, (unresolved) 3JHNHA contributes to the measured linewidth. Second, the dipolar proton environment of each amide proton varies. This causes differences in relaxation rates, R_2 ^1HN - ^1HX . Third, anisotropic rotational diffusion may cause differences in the line widths. Fourth, the amide proton resonances could be life-time broadened by mass exchange with water. Fifth, last but not least, local dynamics could affect the line widths, either by narrowing (fast local dynamics) or broadening (conformational exchange dynamics on the ms –ms timescale), e.g. di-sulfide isomerization, or general conformational flexibility.

We will address these points one by one. Can anisotropic rotational diffusion cause the line width differences? GB1 is an ellipsoid with an long/short axis ratio of 1.8 (Idiyatullin et al., 2003). We calculate from the classical Woessner equations (Woessner, 1962) that R_2 for the ^1HN - ^{15}N dipolar interaction varies +/- 12 % when considering different angles from a relaxation vector to the diffusion axes. But that is for individual relaxation vectors – the ^1HN - ^1HX relaxation vectors contributing to the dipolar R_2 relaxation of a particular ^1HN point in different directions; so, in practice, the small orientational effects will mostly cancel.

The intrinsic (unprotected) amide proton exchange rate is given by the empirical relation (Englander et al., 1972) :

$$k_{ex} = \frac{\ln 2}{200} \left[10^{pH-3} + 10^{3-pH} \right] \times 10^{0.05T} \quad [1]$$

where T is in °C and k_{ex} in min^{-1} .

From the experimental parameters of the spectrum (3 °C, pH 6.5) we calculate from Eq [1] a 0.26 s^{-1} exchange rate, giving rise to a 0.1 Hz life-time broadening for unprotected amide proton resonances. Amide protons engaged in H-bonds within the protein will exchange much slower, with even less broadening. We find that variation in amide proton exchange is not significant for this spectrum.



In principle, the specific proton environment of each amide proton is known from the (high resolution) structure of GB1. Hence, the dipolar R_2 relaxation of ^1HN due to its surrounding protons can be calculated, given the three-dimensional structure.

90 The (unresolved) $^3J_{\text{HN-H}\alpha}$ scalar coupling is also knowable and can be obtained from the structure as well, using the following Karplus equation (Lee et al., 2015)

$$^3J_{\text{HN-H}\alpha} = 8.83 \cos^2(\theta - 60) - 1.29 \cos(\theta - 60) + 0.20 \quad [2]$$

where θ is the dihedral angle spanned by $\text{C}'\text{-N-Ca-C}'$.

95

Summarizing, we have a handle on variables 1 through 4 that affect the ^1HN line width. Hence, making a calculation of these variables, and comparing the resulting calculated linewidth with the experimental (reduced, see below) linewidth, should uncover the presence (or not) of the dynamic properties of the protein, in a sequence-specific fashion.

100



2. Theory of R_2 ^1HN - ^1HX relaxation

Measuring R_2 relaxation in proteins has been taken on by Bodenhausen and co-workers (Boulat and Bodenhausen, 1993) (Segawa and Bodenhausen, 2013). Their work has been focusing on obtaining “pure” R_2 rates for resolved ^1H resonances in
 105 1D NMR spectra, using extremely selective pulses and selective spinlocks. As far as we know, they have not published a linewidth fit of a complete HSQC spectrum, as we are trying to do here.

As virtually all ^1H resonances are resolved in the small proteins GB1 and BPTI, the pure ^1HN - ^1HX R_2 relaxation rate as measured from the cross peaks in a ^{15}N - ^1H HSQC is given by the R_2 relaxation rate for un-like spins (Goldman, 1988)

$$110 \quad R_2^{H(H)} = \frac{1}{20} \left(\frac{\mu_0 \gamma_H \gamma_H \hbar}{4\pi r_{HH}^3} \right)^2 \times \left\{ 5\tau_c + \frac{9\tau_c}{1 + \omega_H^2 \tau_c^2} + \frac{6\tau_c}{1 + (2\omega_H)^2 \tau_c^2} \right\} \quad [3]$$

where μ_0 is the permittivity of space, γ are the gyromagnetic ratios, \hbar Planck’s constant divided by 2π , ω the resonance frequency, and τ_c the rotational correlation time.

Exceptions to equation [3] will arise when the interacting protons have identical chemical shifts (within linewidth). So this may happen for a few ^1HN - ^1HN dipolar pairs. In that case one should use the “identical” equation (Goldman, 1988).

$$115 \quad R_2^{H(H)} = \frac{1}{20} \left(\frac{\mu_0 \gamma_H \gamma_H \hbar}{4\pi r_{HH}^3} \right)^2 \times \left\{ 9\tau_c + \frac{15\tau_c}{1 + \omega_H^2 \tau_c^2} + \frac{6\tau_c}{1 + (2\omega_H)^2 \tau_c^2} \right\} \quad [4]$$

An equation describing a smooth transition between identical and non-identical spins has been given by (Goldman, 1988).

120 However, it is often difficult to measure a “pure” R_2 for HN, because it is affected by anti-phase relaxation due to the scalar-coupled ^1HA (Peng and Wagner, 1992):

$$\sigma^{HN}(t) = H_x^{HN} \cos(\pi J_{HNHA} t) \exp(-R_2^{HN} t) + 2H_y^{HN} H_z^{HA} \sin(\pi J_{HNHA} t) \exp(-(R_2^{HN} + R_1^{HA}) t) \quad [5]$$

and therefore, one measures

$$125 \quad R_2^{HN-eff} = f_{IP} R_2^{HN} + (1 - f_{IP}) * (R_2^{HN} + R_1^{HA}) \quad [6]$$

where f_{IP} is the fraction of time when the coherence is in-phase. In the case of the GB1 HSQC spectrum, where we used a 227 ms t_2 acquisition period, we calculate that for $3J_{HNHA} > 3$ Hz, $(1 - f_{IP})$ is close to 0.5. Hence the R_l rate of the ^1HA does



130 come into play up to 50% and affects the ^1HN linewidth. The key question is now whether the HA R_1 rate is the “selective” or
“unselective” R_1 . For macromolecules, the difference between the rates is very large ($\sim 10\text{ s}^{-1}$ for selective, $\sim 0.2\text{ s}^{-1}$ for
unselective).

The literature is unanimous to state that it is the fast “selective” rate. In the case of (Boulat and Bodenhausen, 1993)’s
careful $^1\text{H R}_2$ measurements, this is certainly the case: they employ extremely selective pulses that excite a single ^1H resonance
in the NMR spectrum. The scalar coupling, if allowed to develop, then affects the z-magnetization of just one other proton.
135 All other ^1H spins are unperturbed as serve as a cross-relaxation bath for that latter proton, driven by the large spectral density
term $J(0)$ (actually $J(|\omega_{\text{HN}} - \omega_{\text{HA}}|)$) (Goldman, 1988):

$$R_1^{\text{HH-SEL}} = \frac{1}{20} \left(\frac{\mu_0 \gamma_H \gamma_H \hbar}{4\pi r_{\text{HH}}^3} \right)^2 \times \left\{ 2\tau_c + \frac{6\tau_c}{1 + \omega_H^2 \tau_c^2} + \frac{12}{1 + (2\omega_H)^2 \tau_c^2} \right\} \quad [7]$$

140 But our case is different. For the ^1HN linewidth in a HSQC, we need to consider the magnetic environment of the scalar
coupled ^1HA during the FID. In fact, all ^1H magnetizations are in the xy plane, and thus saturated, by the last ^1H 90 degree
pulse. Hence the relaxation bath is “hot” and cross relaxation between the ^1HA and other protein protons is expected to be
slow. We should thus expect that the unselective, slow, $^1\text{HA R}_1$ rate is at play in this case (Goldman, 1988):

$$R_1^{\text{HH-UNSEL}} = \frac{1}{20} \left(\frac{\mu_0 \gamma_H \gamma_H \hbar}{4\pi r_{\text{HH}}^3} \right)^2 \times \left\{ \frac{3\tau_c}{1 + \omega_H^2 \tau_c^2} + \frac{24}{1 + (2\omega_H)^2 \tau_c^2} \right\} \quad [8]$$

145 This argument may need refinement. After all, the fast-HSQC experiment we employed, was designed to return the
water magnetization to +z during the FID. Therefore, most of the ^1HA magnetizations will also be in +z and their R_1 rate will
be affected by other aliphatic protons that are saturated. All in all, the situation can become dependent on the detail of the
experiments and chemical shift distributions. In the Results section we will employ a “see what fits best” approach.

150 The entire in-phase / anti-phase and ensuing “selective” / unselective issues is of course moot when one studies
perdeuterated proteins. But there are other methods to avoid the problem. Methods to measure pure R_2 in the presence scalar
couplings have been developed by Bodenhausen and co-workers (Boulat and Bodenhausen, 1993) (Segawa and Bodenhausen,
2013), and by Morris and co-workers (Aguilar et al., 2012). In the original Bodenhausen approach, one obtains a pure HN R_2
when selectively exciting a single amide proton resonance, and selectively spin locking it with a very weak r.f. field.

155 The relaxation rate of that spin-locked resonance is unambiguously described by (Brüschweiler, 1991):



$$\frac{1}{T_{1\rho}} = \frac{1}{20} \left(\frac{\mu_0 \gamma_H \gamma_H \hbar}{4\pi r_{HH}^3} \right)^2 \times \left\{ \frac{5\tau_c}{1 + \omega_{rf-eff}^2 \tau_c^2} + \frac{9\tau_c}{1 + \omega_H^2 \tau_c^2} + \frac{6\tau_c}{1 + (2\omega_H)^2 \tau_c^2} \right\} \quad [9]$$

Here, $\omega_{rf-eff} = \sqrt{\omega_{rf}^2 + \Delta\omega^2}$, where $\Delta\omega$ is the offset between the r.f. carrier and the resonance frequency.

Offset issues also lead to (Massi et al., 2004)

$$R_{1\rho}^{HN-eff} = R_{1\rho} \cos^2 \theta + R_1 \sin^2 \theta \quad [10]$$

160 where $\theta = \arctg\left(\frac{\Delta\omega}{\omega_{rf}}\right)$. (In the Bodenhausen experiment, the r.f. carrier is on the locked resonance, and off-resonance effects do not come into play).

165 However, this experiment is rather impractical for proteins; there is not enough amide proton resolution in the spectrum of even a small protein such as GB1 to select more than a few resonances individually. We are therefore using a variation of this approach. As suggested by Dr. G. Morris (Manchester), we selectively excite all amides, and spin lock them at high power. This avoids the issues with the scalar coupling. Also, because $\omega_{rf-eff}^2 \tau_c^2 \ll 0$, equation [9] becomes identical to equation [3]. Regretfully, it brings in a new issue: are the spin-locked protons relaxing according to the “like” or “unlike” equations? Common wisdom is that since the aliphatic protons are not-spin-locked, amides and aliphatics are “unlike” and follow equation [9]. We had some doubt and elected to test this experimentally. We compared the apparent $R_{1\rho}$ rate for the amide of F52 (9.5 ppm), between two spin-lock fields at 5 kHz and 500 Hz. According to the structure, the dipolar relaxation of this amide is dominated by the HA of residues 52 and 51. Hence the 5 kHz r.f. field “hits” those HA whereas the 500 Hz r.f. field does not. And yet, the $T_{1\rho}$ is identical for both locking fields (see Figure 2) with the same factor of 2.0 drop in intensity between 50 and 75 ms of spinlocking (serendipitous). This convinced us that the excitation profile, and not the locking field strength., determines what are “like” or “unlike” spins.

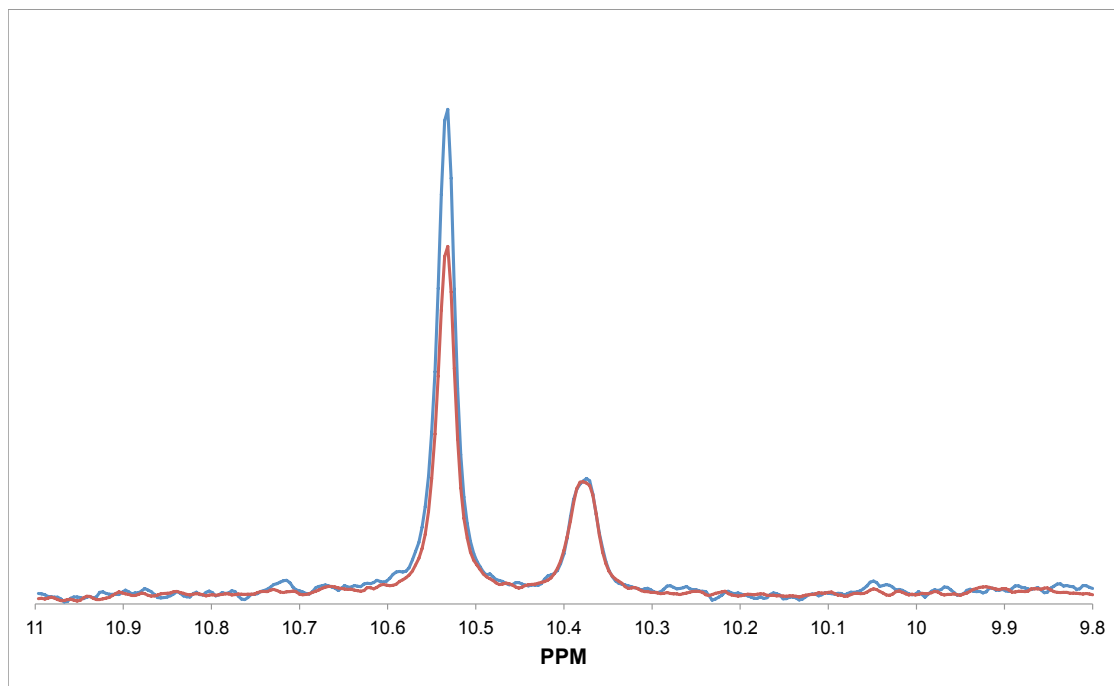


Figure 2A. The peak intensity of Trp43-HE1 (10.53 ppm) and Phe52-HN 10.39 ppm after a 50 ms spinlock (red) and after a 75 ms spinlock (blue), of 5270 Hz, at 10.39 ppm. The red trace was multiplied by 0.5. The $T_{1\rho}$ -HSQC experiment (see supplemental data) was used in 1D mode. The FIDs were multiplied by 5 Hz LB.

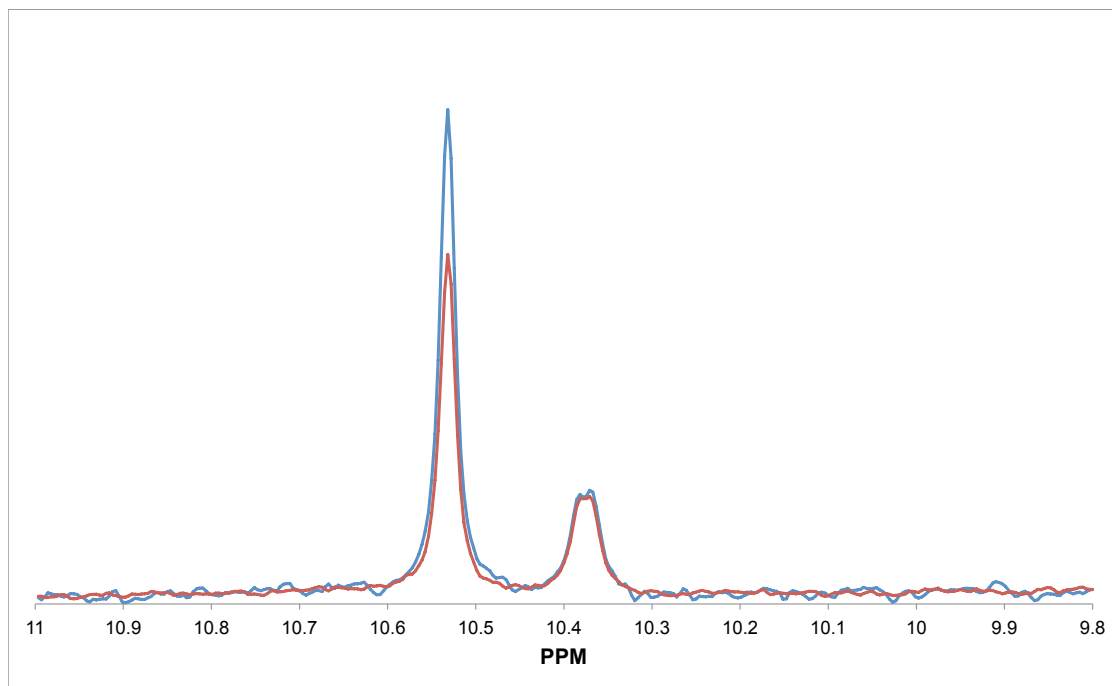


Figure 2B. The peak intensity Trp43-HE1 (10.53 ppm) and Phe52-HN (10.39) ppm after a 50 ms spinlock (red) and a 75 ms spinlock (blue) of 527 Hz, at 10.39 ppm. The red trace was multiplied by 0.5. The $T_{1\rho}$ -HSQC experiment (see supplemental data) was used in 1D mode. The FIDs were multiplied by 5 Hz LB.

180

For those amide protons, for which dipolar partners such as other amide protons, aromatic ring protons, Gln, Asn and Arg sidechain protons are also selected and properly spin-locked, the relaxation will be given by a “like” spin equation (Bothner-By et al., 1984)

185

$$\frac{1}{T_{1\rho}} = \frac{1}{20} \left(\frac{\mu_0 \gamma_H \gamma_H \hbar}{4\pi r_{HH}^3} \right)^2 \times \left\{ \frac{9\tau_c}{1 + \omega_{rf-eff}^2 \tau_c^2} + \frac{15\tau_c}{1 + \omega_H^2 \tau_c^2} + \frac{6\tau_c}{1 + (2\omega_H)^2 \tau_c^2} \right\} \quad [11]$$

With $\omega_{rf-eff}^2 \tau_c^2 \ll 0$ this reduces to the “like” spin relaxation rate [5].



Hence, one can predict with great certainty which equation should be used for which spin-pair. Furthermore, the spin-lock
virtually eliminates broadening by conformational exchange, unless ω_{rf-eff} being in the kHz range, becomes in “resonance”
190 with conformational/chemical exchange processes at the same timescale.
All in all, the theory behind the $T_{1\rho}$ experiment is more robust than the theory behind the cross peak linewidth. Therefore,
we will use the $T_{1\rho}$ experiment and calculations as our departure point for further calculations.

Even in small proteins, many protons interact magnetically. In our programs, described in the appendix, we find
195 typically that 40 protons are present in a 6 Å sphere around an amide proton. All R_2 or $R_{1\rho}$ relaxation rates of these N other
protons j for an amide proton i will co-add if the relaxation vectors ij diffuse independently from each other:

$$R_2^{i-total} = \sum_{j \neq i}^{j=N} R_2^{ij} \quad [12]$$

Taking a larger sphere of interacting protons does not significantly change the summation (see Table S3 in the Supplemental
materials)
200
Obviously, the assumption underlying equation [12] cannot be correct, because the interacting protons in a protein are *not*
diffusing independently. One has to consider dipole-dipole cross-correlated R_2 relaxation (also called relaxation interference).
However, we can show that relaxation interference is almost completely canceled in multi-spin systems, and can be neglected
as a source for large deviations of equation [12] (see Appendix).

205



3. Results and Discussion

Our experimental / computational approach is the following. First we analyze the $T_{1\rho}$ experiments for GB1, and extract the effective rotational correlation time; then we use that correlation time to analyze the GB1 amide proton linewidth and decide, experimentally, whether the R_1 relaxation rate for $^1\text{H}_\text{A}$ contributing to the effective R_2 relaxation rate of $^1\text{H}_\text{N}$ in the HSQC, Equation [6] is (closer) to the “selective” or “unselective” R_1 .

Subsequently, we use what we have learned from GB1 to calculate the HSQC linewidths for BPTI, and analyze the results for dynamical content, and compare with the literature.

3.1 Calibration: GB1 $T_{1\rho}$

For GB1, we collected not only the HSQC spectrum of Figure 1, but also a series of spectra, in which we aim to measure the $^1\text{H}_\text{N}$ $R_{1\rho}$ rate by using an amide-selective excitation pulse followed by a fairly strong spinlock field ($\omega_{rf} = 5.3$ KHz) of varying durations, followed by a HSQC read-out. In this experiment, called semi-selective $T_{1\rho}$ -HSQC, the $^3J_{\text{HNHa}}$ scalar coupling is suppressed. The pulse sequence and the relaxation data obtained are shown in the supplemental materials. With few exceptions, the relaxation data can be fitted with a single exponential with a $R^2 > 0.95$.

For the computations, there are several high-resolution crystal structures 6c9o (V29SeM; 1.2 Å resolution), 6che (A34Sem; 1.1 Å), 6ene (V29SeM; 1.2 Å) and 6cpz (I6Sem; 1.12 Å). SeM is seleno-methionine. Inspection of the structures suggests that the mutation at I6 is the least intrusive on the structure. This mutant is a dimer in the crystal. We use only chain “A” for our calculations. The results for chain “B” are not significantly different. The proton coordinates were added by the routine Molprobit (Williams et al., 2018).

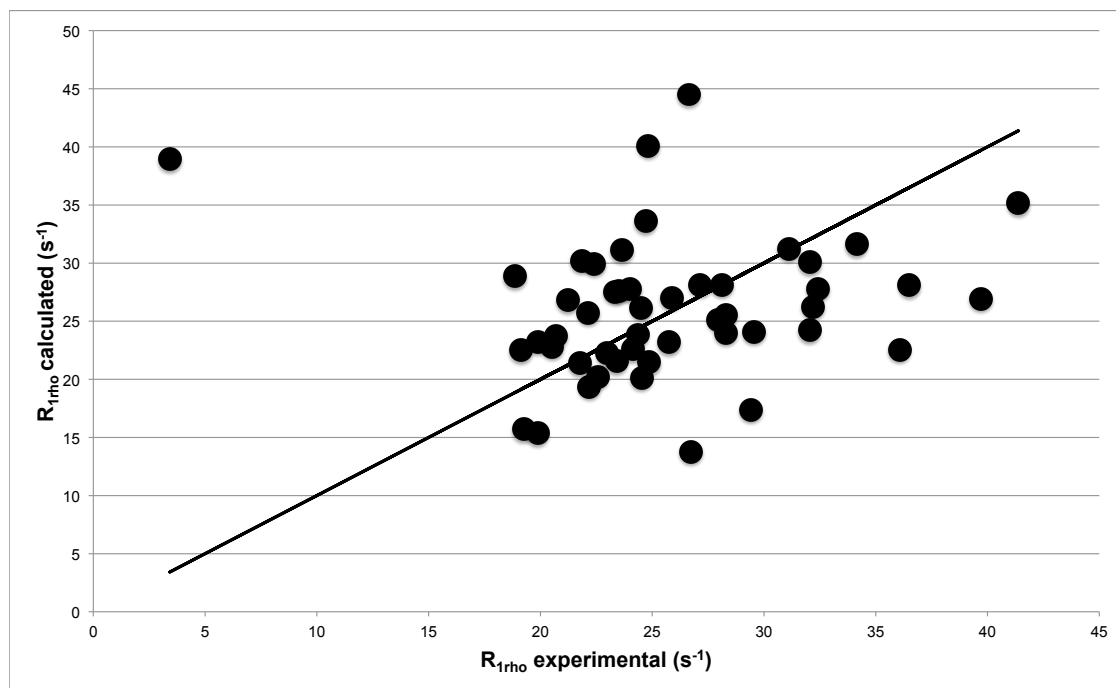
The effective rotational correlation time for the GB1, which is a prolate ellipsoid, was determined to be 6.5 ns from an extensive analysis of ^{15}N relaxation data acquired at 5 °C (Idiyatullin et al., 2003). Using the empirical relation from (Daragan and Mayo, 1997) we extrapolate from the experimental data at 5 °C that $\tau_c = 7$ ns at 3 °C. When using the same empirical equation directly, we find for GB1 that $\tau_c = 8.9$ ns at 3 °C (see also Appendix).

At the outset, we note that by fitting the experimental and calculated $T_{1\rho}$ data, we can only determine an effective rotational correlation time, which is the product $\langle \overline{S_{\text{HN}}^2} \tau_c \rangle$ where the brackets indicate average over residues, and $\overline{S_{\text{HN}}^2}$ is an average order parameter for each $^1\text{H}_\text{N}$ describing the motions of $^1\text{H}_\text{N}$ - $^1\text{H}_\text{X}$ relaxation vectors (in terms of both distance and angular fluctuations).

As a start, we used the 7 ns effective correlation time to compute $R_{1\rho}$ for GB1. The $^1\text{H}_\text{N}$ $R_{1\rho}$ rates due to 6 Å sphere of protons around it, were calculated from equation [9] or [11], depending on whether the other spin was spin locked or not. Because $\omega_{rf}^2 \tau_c^2 \ll 0$ we needed not to concern ourselves with offset effects (see Eq [10]).



The comparison between experimental and calculated $R_{1\rho}$ rates is shown in Figure 3. One sees that the range and median of the computed and experimental $R_{1\rho}$ correspond very well, indicating that we have chosen the correct effective rotational correlation time for the calculations. Actually, we optimized the effective correlation time, by minimizing the RMSD between measured and calculated $R_{1\rho}$. At this point, it is important to recall that we can only optimize the effective correlation time; it may be well the theoretical 8.9 ns multiplied by an $\overline{S_{HN}^2}$ of 0.79. Indeed, one could do more experiments e.g. the analysis of ^{15}N relaxation, to get a better handle on that correlation time, but, as explained in the introduction, we would like to find a way to obtain dynamical information without such experiments. While the range of calculated and experimental $R_{1\rho}$ rates correspond well, the actual correlation is poor. For calculated data points larger than the experimental ones can be explained by low order parameters. Experimental data points larger than computed ones are harder to explain. In $T_{1\rho}$ the latter cannot be, in general, caused exchange broadening, as it is suppressed by the spin lock. For now we chose not to be concerned by these issues as we want to use the experiment to help us decide the (effective) rotational correlation time.



250

Figure 3. Experimental (600 MHz) and calculated $R_{1\rho}$ rates for the ^1HN resonances of GB1, at 30°C . The line $y=x$ is shown. The calculations were based on structure 6cpz, using an effective correlation time of 7 ns.



3.2 Calibration: GB1 HSQC

255 With the $R_{1\rho}$ data analyzed and the effective correlation time estimated, we turn our attention to the HSQC spectrum
itself. The HSQC spectrum in Figure 1, processed with 1 Hz exponential window in t_2 , shows many of the $^3J_{\text{HNHA}}$ scalar
couplings, which closely correspond to the scalar couplings we compute from the crystal structure using the Karplus equation
[2]. The Sparky software (Goddard and Kneller, 2000) does not fit resolved doublets as a pair, but as a single resonance, as
shown in the cross sections shown in Figure 1. The fits, using a Gaussian lineshape, were individually inspected and found to
260 be excellent, with an estimated uncertainty of less than a 1 Hz.

Before we can make comparisons between experimental R_2 and computed R_2 data, we have to correct the measured
 ^1HN line widths for several effects. First, we subtract the computed scalar couplings. Second, we need to consider ^1HN dipolar
relaxation due to the amide nitrogen, chemical shift anisotropy relaxation and field inhomogeneity. We calculate that for τ_c
 $=7$ ns, the ^1HN dipolar interaction with ^{15}N accounts for ~ 2 Hz, that the ^1H CSA contributes ~ 0.2 Hz at 600 MHz (using CSA
265 values from (Loth et al., 2005)), while field inhomogeneity typically is limited to 1 Hz. We decoupled ^{13}CO during data
acquisition, but the $^2J_{\text{HNCA}}$ of 2 Hz (Schmidt et al., 2011) should also contribute to the ^1HN linewidth. We thus are inclined to
subtract 5 Hz from the apparent experimental ^1HN line widths in addition to the 1 Hz due to the window function (total 6 Hz).
What is left is what we call the “reduced experimental line width”, which *should* consist of just the sum of the ^1HN - ^1HX dipolar
line widths, affected by antiphase relaxation due to the $^3J_{\text{HNHA}}$ and potentially affected by the fast and/or slow dynamics we
270 try to uncover. However, we find, by simulation, that unresolved scalar couplings add a full 1 Hz less to the linewidth than
expected. When assuming that the instrument was well-shimmed, it is thus reasonable to estimate that one should subtract just
2-3 Hz from the observed linewidths. We will determine what is best from the calculations.

For Figure 4 we used Equations 3, 6 7 and 8, with the effective $\tau_c = 7$ ns obtained by the $T_{1\rho}$ experiments taking
275 into account all protons in a sphere of 6 Å around the individual amide protons. We compute the selective and unselective
 $R_{1\text{HA}}$ also from all ^1HA - ^1HX interactions within 6 Å in the crystal structure, co-adding all relaxation rates [7], not taking into
account cross correlated relaxation on basis of the same arguments outlined for R_2 (see Appendix). The fractions in-phase for
Equation [6] were calculated from the calculated scalar couplings and the acquisition time (227 ms), and were found to vary
between 0.43 and 0.65. Hence taking the antiphase relaxation into account is necessary.

280

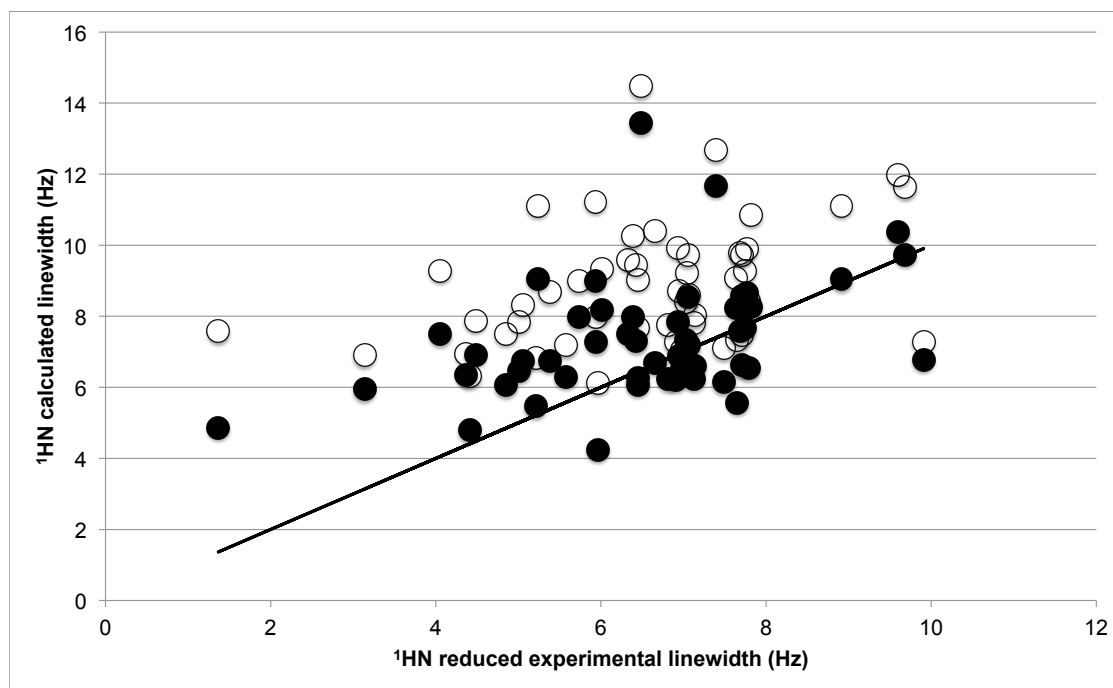


Figure 4A. Calculated ^1HN linewidths for GBI, using Equations 3 and 6, $\tau_c = 7 \text{ ns}$

The experimental linewidth was reduced by the scalar couplings and 3 Hz (see text).

For the filled circles, we used the “unselective” $^1\text{HA } R_1$ (Eq 8). The RMSD with the experimental values is 1.91 Hz. For the open circles we used the “selective” $^1\text{HA } R_1$ (Eq 7).

The RMSD with the experimental values is 3.0 Hz.

285

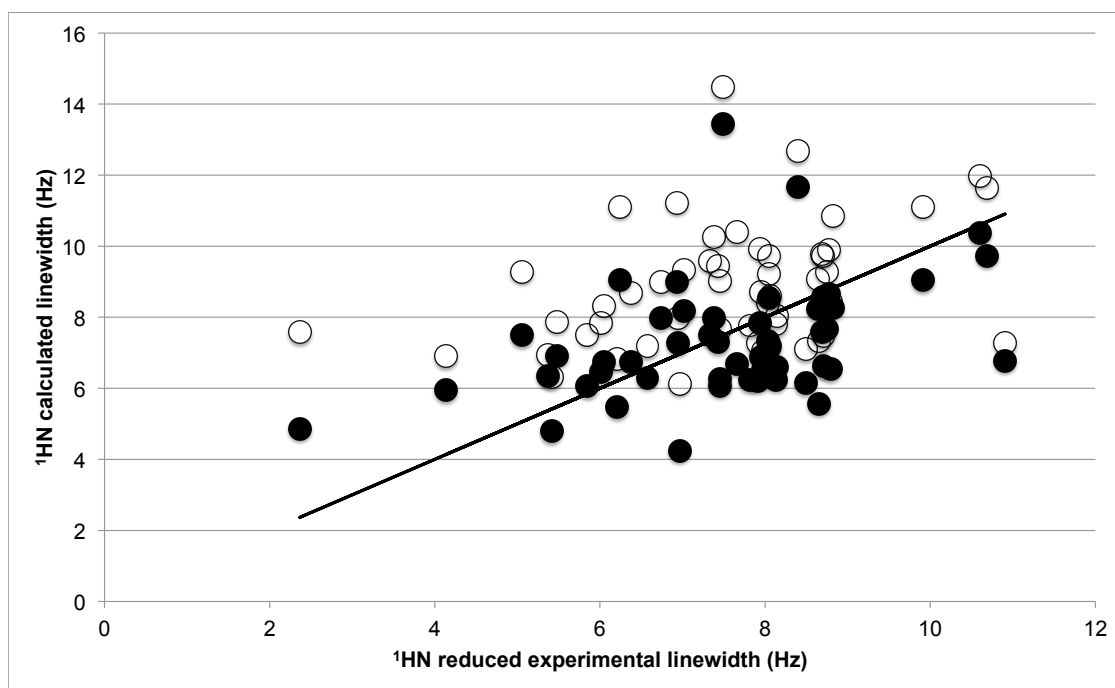
In Figure 4A we show the results of these calculations. For panel A, we subtracted 3 Hz from the experimental linewidth (in addition to $^3\text{J}_{\text{HNHA}}$) as outlined above. It is clear that, when doing that, the linewidths calculated taking the unselective HA R_1 into account (filled circles), are on average too large (RMSD 1.91 Hz). It is also clear that the calculations using the selective HA R_1 into account turn out worse (open circles; RMSD 3.00). For Figure 4B, we subtracted just 2 Hz from the experimental linewidth (in addition to $^3\text{J}_{\text{HNHA}}$). Now the median value of the “unselective” calculation corresponds better to that of the reduced experimental values and we obtain a RMSD of 1.75 Hz. For the “selective” calculation we obtain RMSD 2.29 Hz.

290

This is what we set out to resolve. The theory (and my consultancies with several colleagues) does not establish unambiguously which HA R_1 rate is to be used; but the comparison between experiment and calculation does. Clearly, we



295 need the “unselective” $^1\text{H}_A R_1$ in this experiment. In practice, this rate is so small, that the anti-phase relaxation is within a few tenths of s^{-1} within the in-phase rate. Hence, we do not need to worry about in-phase / anti-phase issues. The situation will be different when using a HSQC pulse sequence using selective amide proton pulses throughout, not exciting anything else (Gal et al., 2007). In that case, the scalar-coupling-induced $^1\text{H}_A$ z-magnetization perturbation during the FID would be in an unperturbed aliphatic spin bath, and the fast “selective” $^1\text{H}_A R_1$ would be in effect.



300

Figure 4B. Calculated $^1\text{H}_N$ linewidths for GB1, using Equations 3 and 6, $\tau_c = 7 \text{ ns}$
The experimental linewidth was reduced by the scalar couplings and 2 Hz (see text).
For the filled circles, we used the “unselective” $^1\text{H}_A R_1$ (Eq 8). The RMSD with the experimental values is 1.75 Hz. For the open circles we used the “selective” $^1\text{H}_A R_1$ (Eq 7). The RMSD with the experimental values is 2.29 Hz.

305

As explained before, we cannot determine a real correlation time from this fitting procedure. Rather we determine the product

$\left\langle \overline{S_{HN}^2} \tau_c \right\rangle$ to be 7 ns. If we take $\tau_c = 8.9 \text{ ns}$ at 3°C as calculated from the empirical relation (Daragan and Mayo, 1997) for



310 τ_c , we would obtain that $\overline{S_{HN}^2}$ equals 0.79. Parenthetically, we note that we have independently carried out an analysis of protein rotational correlation times as available in the literature, and found those to closely follow the empirical relation (Daragan and Mayo, 1997) (see appendix).

315 How does the estimated $\overline{S_{HN}^2}$ compare with literature values? Obviously, there are no such values determined, but there is an comprehensive paper of (Idiyatullin et al., 2003) calculating ^{15}N order parameters using several different approaches. Using the extended Modelfree method (Clare et al., 1990), they obtain an average order parameter of 0.70, while using their own method, they obtain an average of 0.62. From this it is suggested that GB1 is a rather dynamical molecule, and one may argue that one sees that back in the ^1HN relaxation as well. However, we note that (Idiyatullin et al., 2003) obtain a rotational correlation time τ_c for the GB1 prolate ellipsoid of 6.5 ns from the ^{15}N relaxation data acquired at 5 $^{\circ}\text{C}$, while the empirical relation from the same lab would predict τ_c 8.6 ns. Even so, both methods point to a quite dynamic GB1 protein, even at temperatures as low as 3 $^{\circ}\text{C}$.

320 In summary, for GB1, we have established by comparing $T_{1\rho}$ and HSQC linewidth data, that one can compute a reasonable range of ^1HN R_2 rates using just a single equation for unlike spins. When assuming a rotational correlation time as predicted by the literature, we *predict* from comparing the calculated and experimental ^1HN linewidths that the average ^1HN - ^1HA order parameter must be 0.79, indicating much internal motion. Others have come to similar conclusions analyzing ^{15}N relaxation data (Idiyatullin et al., 2003). With this, we have arrived at our goal: we show that we *can* extract motional information from the ^1HN linewidths in a HSQC spectrum by making simple calculations based on a crystal structure. In the case of GB1 this is overall motional narrowing. In BPTI, as we will see below, we can also extract conformational exchange line broadening that is not immediately apparent from the spectrum itself.

330



3.3 Application: BPTI

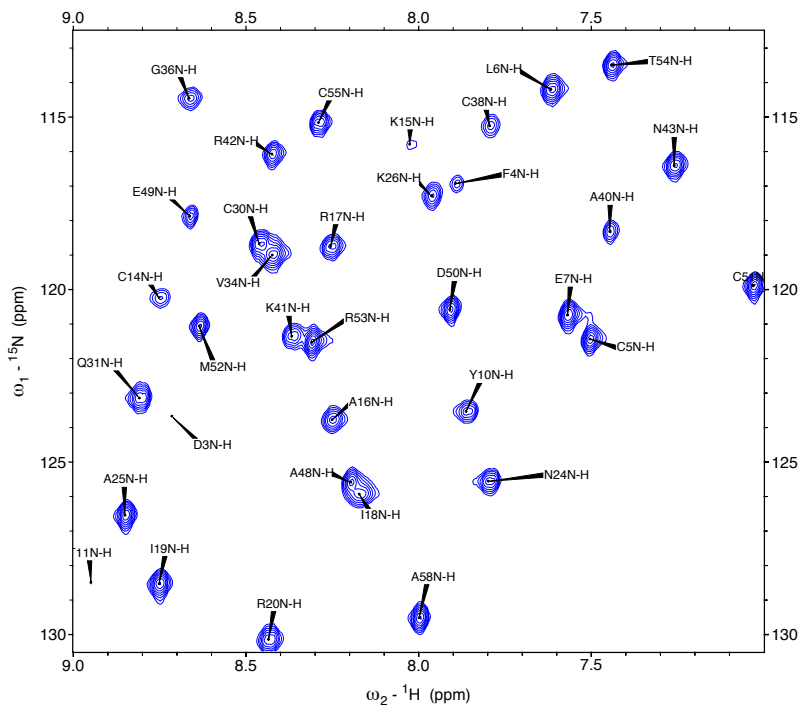


Figure 5. Section of a 500 MHz ^{15}N - ^1H HSQC for BPTI, 30 °C, pH 5.8 , processed with a 1Hz exponential window in t_1 and t_2 .

335

Assignments and the time-domain data for a ^{15}N - ^1H HSQC spectrum of bovine trypsin inhibitor (BPTI) recorded at 30 °C, pH 5.8 are available at the Biological Magnetic Resonance Bank, while a 1.3 Å resolution crystal structure (9PTI.PDB) is available in the Protein Data Bank. We processed the time-domain data with a 1 Hz exponential window in t_2 . At the contour level of Figure 5, several peaks are missing, indicating intensity dispersion. Table S2 shows a 30-fold range for S/N and an 8-fold range for the linewidth, much more than for GB1. Significantly, and in contrast to GB1 at 3 °C, this processed spectrum does *not* show any resolved $^3\text{J}_{\text{HNHA}}$ couplings at 30 °C. Nevertheless, the protein is not perdeuterated. According to three sources, the correlation time should be between 2.5 and 3.5 ns, much less than the 7 ns correlation time of GB1 at 3 °C. (Beeser et al., 1997),(Daragan and Mayo, 1997) and (Sareth et al., 2000). Why are these doublets missing? From Equation [1] we calculate a 1.15 s^{-1} mass exchange rate, giving rise to maximum broadening of $\sim 0.4 \text{ Hz}$ for unprotected amide proton resonances, so that cannot be the reason. We can, a priori, already assume that the sample must have been aggregated. Indeed, MRD studies suggest that, at high concentrations, BPTI can form decamers in solution (Gottschalk et al., 2003). As it turns

345

out, this sample of BPTI mimics a much larger molecule, and provides an excellent opportunity to test our method on a “large” protein.

350 In Figure 6, we show the comparison of experimental and calculated ^1HN linewidths for BPTI. We subtracted, besides the calculated scalar couplings, 2 Hz from the linewidths as reported by Sparky (^{15}N -H dipolar, ^1HN CSA and shimming). For the calculations we just used Equation [3], taking into account all protons in a sphere of 6 Å around the individual amide protons. The use of just Equation 3 is justified by the fact that the HNHA anti-phase R_2 relaxation rate is virtually identical to the in-phase HN R_2 rate (see the discussion for GB1). We iterated the (unknown) rotational correlation time and found a best
355 fit for $\tau_c = 6.3$ ns.

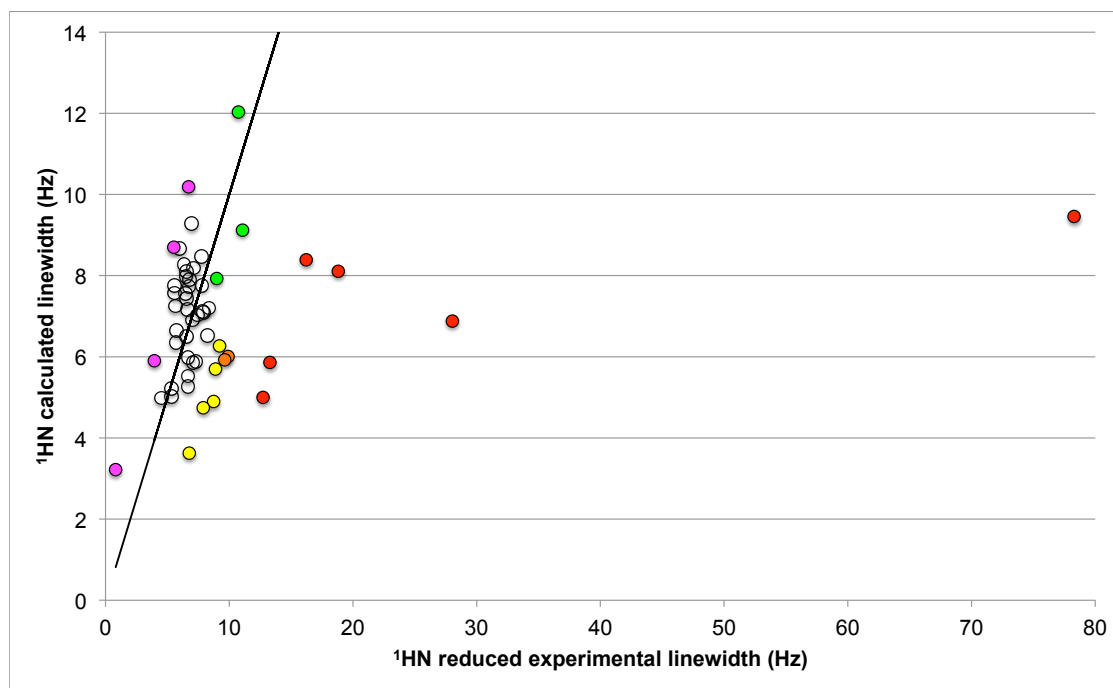


Figure 6A. Calculated ^1HN linewidths for BPTI, using Equation 3, $\tau_c = 6.3$ ns.

The experimental linewidth was reduced by the scalar couplings and 2 Hz (see text).

The drawn line has a slope of 1. Color coding: Red: D3, T11, C14, K15, G37 and K46. Orange: A16, A40.

Yellow: F4, Y10, C38, N44. Green: Y21, G36, G57. Magenta, I19, L29, Y35, R42 and A58.

360

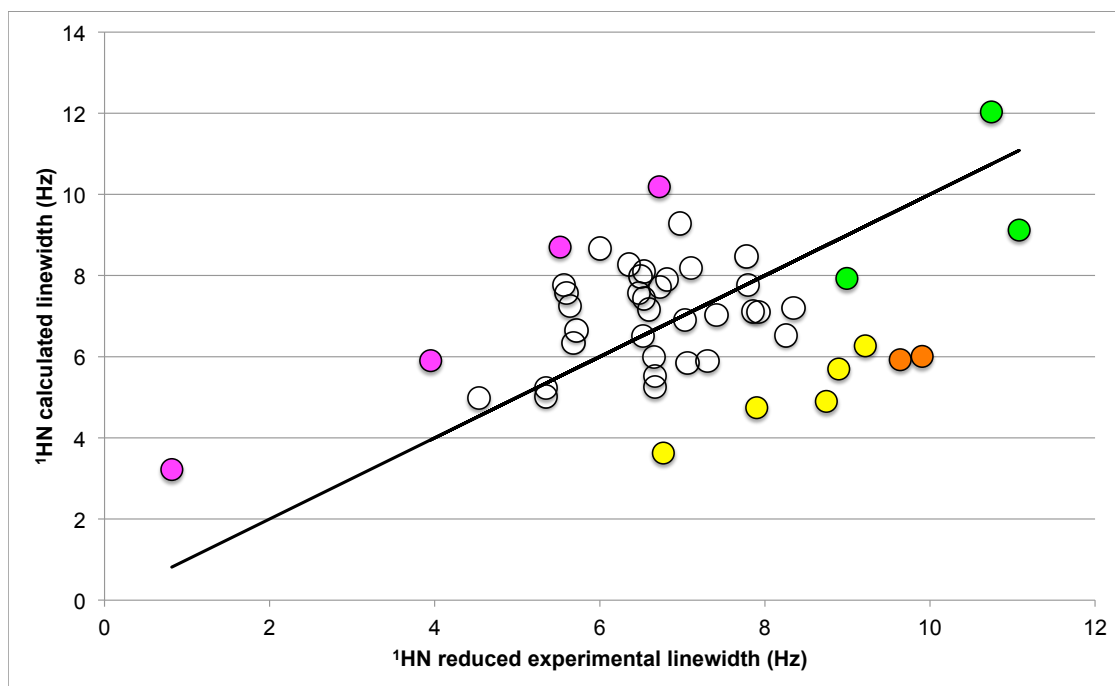


Figure 6B. Enlargement of Figure 6A. Calculated ^1HN linewidths for BPTI, using Equation 3, $\tau_c = 6.3$ ns. The experimental linewidth was reduced by the scalar couplings and 2 Hz (see text). The drawn line has a slope of 1. Color coding: Orange: A16, A40. Yellow: F4, Y10, C38, N44. Green: Y21, G36, G57. Magenta, I19, L29, Y35, R42 and A58.

365

In the ^1HN linewidth data by itself (i.e. Figure 6A projected on the x-axis), one finds already ample indication of conformational exchange broadening. The red data points for D3, T11, C14, K15, G37 and K46. stand out with linewidths upto 80 Hz. Indeed, for red points one does not need a calculation to decide if these resonances are conformationally exchange broadened. In Figure 7, we show the crystal structure of BPTI, where we use the same color coding as in Figure 6.

370

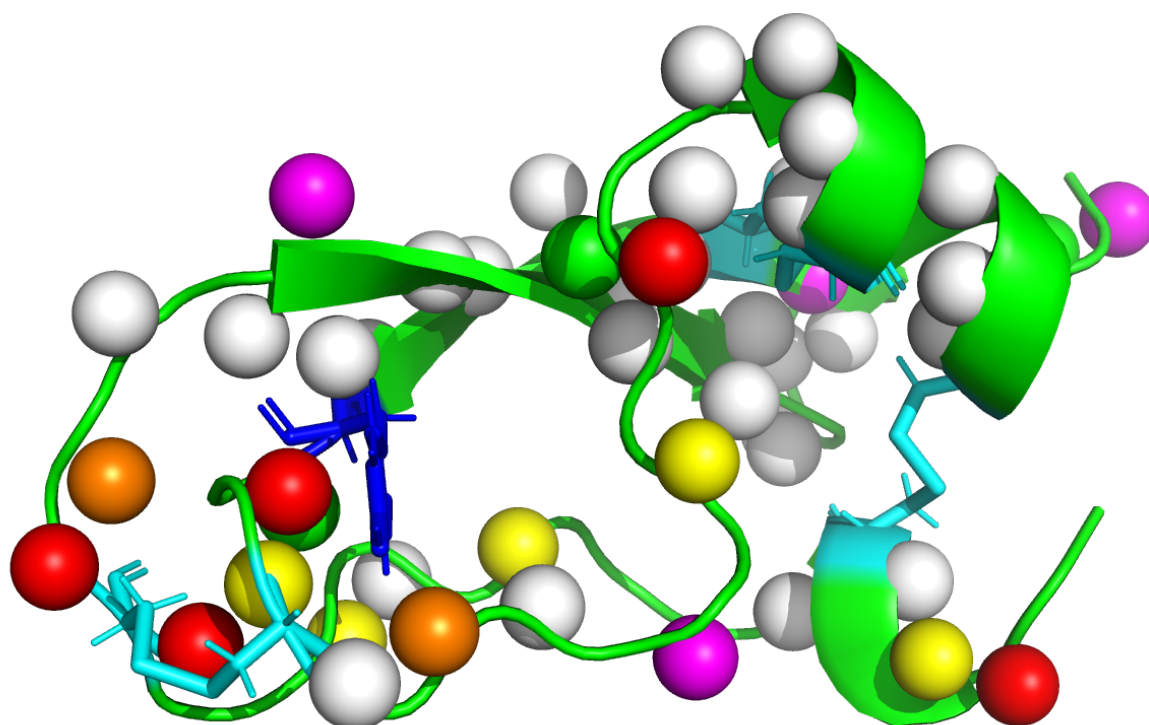


Figure 7A. Crystal structure of BPTI (9pti) with amide protons (spheres) color coded as in Figure 6A. Disulfide bridges are shown in cyan. Tyr35 is shown in blue.

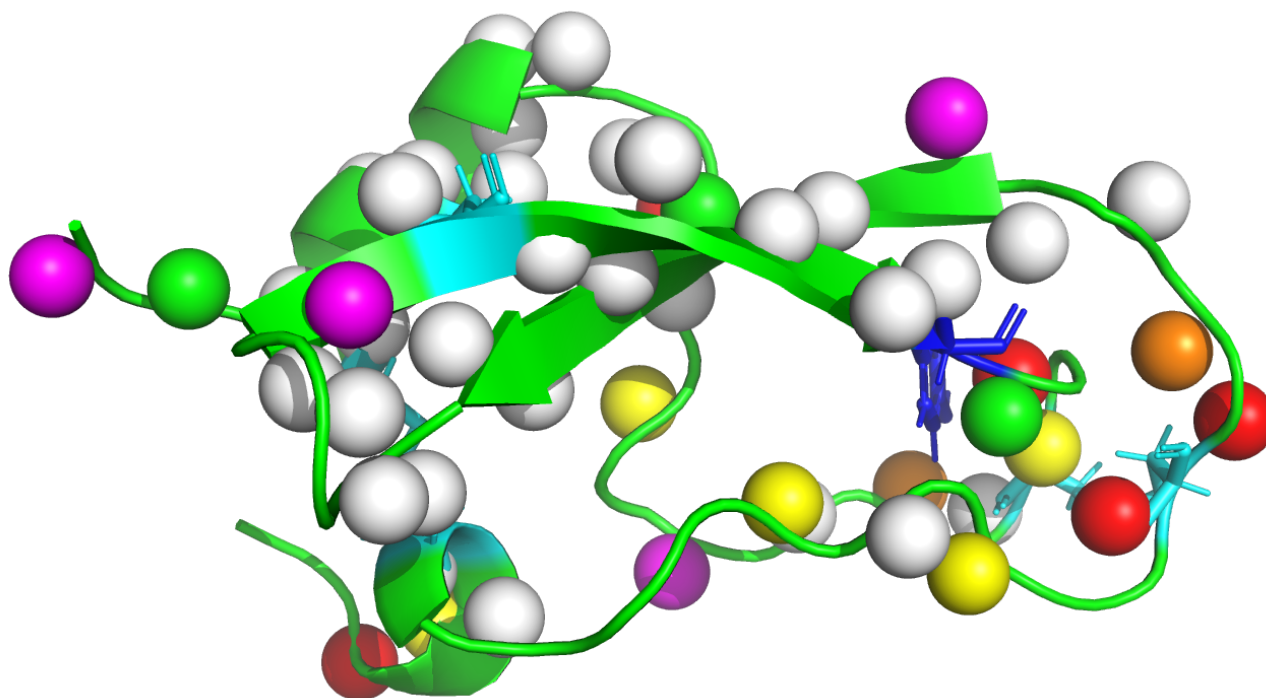


Figure 7B. As Figure 7A, rotated 180 degrees along the vertical axis.

375 Three of five excessively broadened resonances belong to region in the left bottom of protein in Figure 7A. This protein area
comprises two anti-parallel beta strands with residues 10-15 and 36-40, and harbors the Cys14 – Cys38 disulfide. Returning
to Figure 6, one would be hard-pressed to declare the orange points as exchange broadened or not. They are on the edge of the
bulk of the distribution. But the calculated data for these points is just 6 Hz; this helps in deciding the matter, suggesting that
the experimental data are exchange broadened. The two orange points correspond to A16 and A40, which, significantly, are
380 in the same area where the red points are in Figure 7A. From the five yellow points in Figure 6 three map in the same area
again (10, 12, 38), one is residue Phe4 next to the excessively broad Asp3 (bottom right of Figure 7A). This broadening is
likely amine-catalyzed amide proton mass exchange life-time broadening which is so often seen for the N-terminal 3 to 4
residues in proteins. The last yellow point at 6.8 ppm belongs to N44.

The majority of the broadened ¹H_N resonances belonging to the red, orange and yellow data points in Figure 6B are
385 clustered and are not all over the protein. Just by itself, this result suggests that our calculation and its interpretation give rise



to a useable results. But there is more. In early work, (Szyperski et al., 1993) detected ^{15}N exchange broadening for residues 14-16 and 38-39 in BPTI. Our current calculations (Figures 6 and 7) point to exactly the same area. (Szyperski et al., 1993) suggest that the ^{15}N exchange broadening is a result of the Cys14 – Cys38 disulfide isomerization at a stochastic rate of 500 s^{-1} and a superposed conformational process of the entire area with a stochastic rate $> 10,000\text{ s}^{-1}$. If we assume that the changes in chemical shift associated with these conformational changes are the same for ^{15}NH and ^1HN in terms of ppm, we would expect the 500 s^{-1} process to give rise to slow exchange or resonance doubling in ^1H , which is not observed. Hence it is likely that the ^1HN line widths are sensitive to the faster process.

The effect of mutations on the ^{15}N relaxation of BPTI has also been studied. According to (Beeser et al., 1997), fast and slow dynamics is mostly absent in wt-BPTI, with order parameters between 0.8 and 0.9 (except for the C-terminus) and very little exchange broadening ($\sim 1\text{ Hz}$), except for two areas (again) 14-15 and 38-40. (See Figure 4A of (Beeser et al., 1997)). This is in agreement with the data of (Szyperski et al., 1993). The effect of the mutation Tyr35Gly on ^{15}N the relaxation parameters was also studied; it exacerbates the broadening in magnitude (up to $\sim 3\text{ Hz}$) and extent (comprising residues 10-20 and 32-43), (see Figure 4B in (Beeser et al., 1997)). We show Tyr35 in Figure 7. Interestingly, our ^1H dynamic results also comprise that same *extended* area; it thus seems that the ^1HN resonances are sensitive to extended dynamical processes present in the wild-type protein, that are only observable by ^{15}N relaxation after a (predictably) destabilizing mutation.

There are several points that are calculated to be significantly broader than the experiment; these data points are shown in magenta. They comprise I9, L29, R42 and A58. Such outliers would indicate resonances that according to the crystal structure coordinates should be broad (a dense proton environment), but are not broad in the experimental data. That would suggest fast local motion. The ^{15}N order parameter for Ala58 is small ((Beeser et al., 1997)), which would corroborate the finding here. However, the ^{15}N -relaxation data does not show reduced order parameters for I9, L29 and R42. This maybe a genuine difference in ^{15}N and ^1HN order parameters, or noise. We also have no quick rationale for the experimental broadening for Lys 46 (red, on the top-middle of Figure 7A) and the calculated rate for Asn 44 (yellow, just below it). Previous work ^{15}N relaxation work does not show anything particular for these residues. But, the resonance of K46 is actually missing at the contour level of the spectrum in Figure 5; so there is no question that something is going on there. We may speculate that small motions of the ring of Phe45, which hovers above amides 44 and 46, can translate in changing ring-current shifts, causing broadening for these resonances, which is not due to an actual spatial change at the level of the amides themselves. A ring-current-driven mechanism could be consistent with the lack of broadening effects in the ^{15}N spectral data: ring current effects are, as expressed in Hz, 10 times larger for ^1H than for ^{15}N . Hence, varying ring current shifts are apt to cause much more “conformational” exchange broadening for ^1HN than for ^{15}NH . Last, there are three points Y21, G36 and G57, colored green. The calculations identify them as broad as well, suggesting that the broad linewidth is intrinsic. According to the ^{15}N data, no broadening is occurring for those residues either. It is significant for assessing the value of our calculations, that the two right-most green points in Figure 6B (G36 and G57) would be identified as exchange broadened from the experimental ^1HN linewidth distribution, but that the calculations indicate that they are not.



420 But how do we do with our calculations *within* the bulk of the distribution? Figure 6B shows that it is not good at all
and not much worse than for GB1 (Figure 4B). There is hardly a correlation between experiment and calculation – the
calculated values all lie around 7 Hz, while the experimental values vary almost a factor of two. At the moment we have no
explanation for this, merely suggesting that there is much room for improvement, likely in measuring / calculating the ^1HN -
 ^1HX order parameters. We note that we used a BPTI crystal structure with 1.2 Å resolution, which has a coordinate precision
of ~ 0.2 Å (DePristo et al., 2004). This can give rise to considerable errors in R_2 calculations. For example, a HN(i) to HA(i-
425 1) distance of nominally 2.2 Å in a beta sheet structure (Wüthrich, 1986) may be incorrect by 9%, and produce a 68% error
for the R_2 relaxation contribution. There is work to be done here, for sure. Nevertheless, just considering the *outliers* of the
distribution appears to result in relevant dynamical information.

430



4. Conclusion

We developed computer programs to predict amide proton line widths from (crystal) structures. We calibrate our programs by comparing computational and experimental results for GB1, using ^{15}N - ^1H HSQC and semi-selective $T_{1\rho}$ experiments. We find that we can predict the correct range of ^1HN R_2 relaxation rates from a crystal structure using a Karplus equation and a program based on just one relaxation equation. We deduce that GB1 has fairly low average ^1HN order parameters (0.8), in broad agreement with what was found by others from ^{15}N relaxation experiments. We apply the program to the BPTI crystal structure and compare the results with a ^{15}N - ^1H HSQC spectrum of BPTI. After adjusting the correlation time, we find from the outliers in the distribution a cluster of conformationally broadened ^1HN resonances that belong to an area for which broadened ^{15}NH resonances have been previously reported. Thus, our approach can yield important dynamical data. We feel that this approach may be useful to glean insights into the dynamical properties of larger biomolecules for which high-quality ^{15}N relaxation data cannot be recorded. The semi-selective $T_{1\rho}$ experiments are also not difficult to perform and are also suitable for application to larger molecules. Comparing these relaxation data ($T_{1\rho}$ and the ^1HN linewidth) for proteins in different states or complexation forms, is likely much more interesting. Perhaps the dynamical differences can be tied to functional properties, as has been carried before for small proteins, but much less so for the larger ones. The theory of ^1HN R_2 for proteins is not iron-clad; issues such as “like” and “unlike” R_2 , “in-phase/antiphase” relaxation, “selective” and “unselective” R_1 rates and cross-correlated R_2 relaxation all play roles in these issues. As a by-product of our “calibration” work for GB1, we help resolve most of those (sometimes contentious) issues.

5. Acknowledgements

Dr. Gottfried Otting has graciously provided me with remote instrument time at the Canberra NMR facility, and the use of his sample of ^{13}C , ^{15}N labeled GB1. I thank Professor Arno Kentgens (Nijmegen) for helpful discussions on solid state NMR powder patterns. I have taken advice from Professors Raphael Bruschweiler (Ohio State), Gareth Morris (Manchester) and Drs. Ad Bax (Bethesda), Bernhard Brutscher (Grenoble) and Anaya Majumdar (Baltimore).

455

6. Code/Data availability.

The Fortran90 computer codes are available from the author and will be deposited at <https://github.com>.

The (Bruker) data directories for the GB1 experiments will be deposited at the Biological Magnetic Resonance Bank.

7. Author contributions.

ERPZ conceived and wrote the paper. He wrote all computer codes and remotely carried out the GB1 NMR experiments.

8. Conflicting interests

None.



465

9. Supplemental materials

Tables with Sparky linewidth/integration lists for GB1 and BPTI, as well as data fits for the semi selective $T_{1\rho}$ experiments, as well the pulse sequence for that experiment, are given in the Supplemental Materials.



470 10. References

- Aguilar, J. A., Nilsson, M., Bodenhausen, G., and Morris, G. A.: Spin echo NMR spectra without J modulation, *Chem. Commun.*, 48, 811-813, 2012.
- Akke, M., Bruschweiler, R., and Palmer, A. G.: NMR Order Parameters and Free-Energy - an Analytical Approach and Its Application to Cooperative Ca²⁺ Binding by Calbindin-D(9k), *J. Am. Chem. Soc.*, 115, 9832-9833, 1993.
- 475 Beeser, S. A., Goldenberg, D. P., and Oas, T. G.: Enhanced protein flexibility caused by a destabilizing amino acid replacement in BPTI, *Journal of molecular biology*, 269, 154-164, 10.1006/jmbi.1997.1031, 1997.
- Bertelsen, E. B., Chang, L., Gestwicki, J. E., and Zuiderweg, E. R. P.: Solution conformation of wild-type E. coli Hsp70 (DnaK) chaperone complexed with ADP and substrate, *Proceedings of the National Academy of Sciences of the United States of America*, 106, 8471-8476, 10.1073/pnas.0903503106, 2009.
- 480 Bothner-By, A. A., Stephens, R. L., Lee, J., Warren, C. D., and Jeanloz, R. W.: Structure determination of a tetrasaccharide: transient nuclear Overhauser effects in the rotating frame, *J. Am. Chem. Soc.*, 106, 811-813, 1984.
- Boulat, B., and Bodenhausen, G.: Measurement of proton relaxation rates in proteins, *J. Biomolecular NMR*, 3, 335-348, 1993.
- Brüschweiler, R. P.: Structural dynamics of biomolecular monitored by nuclear magnetic resonance relaxation, ETH Zurich, Zurich, 1991.
- 485 Clore, G. M., Szabo, A., Bax, A., Kay, L. E., Driscoll, P. C., and Gronenborn, A. M.: Deviations from the Simple 2-Parameter Model-Free Approach to the Interpretation of ¹⁵N Nuclear Magnetic-Relaxation of Proteins, *J. Am. Chem. Soc.*, 112, 1990.
- Copié, V., Battles, J., Schwab, J., and Torchia, D.: Secondary structure of β-hydroxydecanoyl thiol ester dehydrase, a 39-kDa protein, derived from Hα, Cα, Cβ and CO signal assignments and the Chemical Shift Index: Comparison with the crystal structure, *Journal of Biomolecular NMR*, 7, 335-340, 10.1007/BF00200435, 1996.
- 490 Daragan, V. A., and Mayo, K. H.: Motional model analyses of protein and peptide dynamics using ¹³C and ¹⁵N NMR relaxation, *Prog. NMR Spectrosc.*, 31, 63-105, 1997.
- de la Torre, J. C., Huertas, M. L., and Carrasco, B.: HYDRONMR: Prediction of NMR Relaxation of Globular Proteins from Atomic-Level Structures and Hydrodynamic Calculations, *J. Magn. Reson.*, 147, 138-146, 2000.
- DePristo, M. A., de Bakker, P. I. W., and Bludell, T. L.: Heterogeneity and inaccuracy in protein structures solved by X-ray crystallography, *Structure*, 12, 831-838, 2004.
- 495 Englander, S. W., Downer, N. W., and Teitelbaum, H.: Hydrogen exchange, *Annual review of biochemistry*, 41, 903-924, 10.1146/annurev.bi.41.070172.004351, 1972.
- Fischer, M. W. F., Majumdar, A., and Zuiderweg, E. R. P.: Protein NMR relaxation: theory, applications and outlook, *Prog. NMR Spectrosc.*, 33, 207-272, 1998.
- 500 Gal, M., Schanda, P., Brutscher, B., and Frydman, L.: UltraSOFAST HMQC NMR and the Repetitive Acquisition of 2D Protein Spectra at Hz Rates, *J. Am. Chem. Soc.*, 129, 1372-1377, 2007.
- Gardner, K., Zhang, X., Gehring, K., and Kay, L.: Solution NMR Studies of a 42 KDa Escherichia Coli Maltose Binding Protein/Cyclodextrin Complex: Chemical Shift Assignments and Analysis, *J Am Chem Soc*, 120, 11738-11748, 1998.
- Gardner, K. H., Rosen, M. K., and Kay, L. E.: Global folds of highly deuterated, methyl-protonated proteins by multidimensional NMR, *Biochemistry*, 36, 1389-1401, 1997.
- 505 Goddard, T. D., and Kneller, D. G.: SPARKY 3, University of California, San Francisco, 2000.
- Goldman, M.: Interference effects in the relaxation of a pair of unlike spin 1/2 nuclei, *J. Magn. Reson.*, 60, 437-452, 1984.
- Goldman, M.: Quantum Description of High-Resolution NMR in Liquids, Clarendon Press, Oxford, 1988.
- Gottschalk, M., Venu, K., and Halle, B.: Protein self-association in solution: the bovine pancreatic trypsin inhibitor decamer, *Biophysical journal*, 84, 3941-3958, 10.1016/s0006-3495(03)75122-4, 2003.
- 510 Idiyatullin, D., Daragan, V. A., and Mayo, K. H.: 15NH Backbone Dynamics of Protein GB1: Comparison of Order Parameters and Correlation Times Derived Using Various "Model-Free" Approaches, *J. Phys. Chem. B*, 107, 2602-2609, 2003.
- Kay, L. E., Torchia, D. A., and Bax, A.: Backbone dynamics of proteins as studied by ¹⁵N inverse detected heteronuclear NMR spectroscopy: application to staphylococcal nuclease, *Biochemistry*, 28, 8972-8979, 1989.
- 515 Kay, L. E.: Protein dynamics from NMR, *Biochem Cell Biol*, 76, 145-152, 10.1139/bcb-76-2-3-145, 1998.
- Korzhnev, D. M., Kloiber, K., Kanelis, V., Tugarinov, V., and Kay, L. E.: Probing slow dynamics in high molecular weight proteins by methyl-TROSY NMR spectroscopy: application to a 723-residue enzyme, *J Am Chem Soc*, 126, 3964-3973, 2004.
- Lee, A. L., Kinnear, S. A., and Wand, A. J.: Redistribution and loss of side chain entropy upon formation of a calmodulin-peptide complex, *Nat. Struct. Biol.*, 7, 72-77, 2000.



- 520 Lee, J. H., Li, F., Grishaev, A., and Bax, A.: Quantitative residue-specific protein backbone torsion angle dynamics from concerted measurement of 3J couplings, *J Am Chem Soc*, 137, 1432-1435, 10.1021/ja512593s, 2015.
Loth, K., Pelupessy, P., and Bodenhausen, G.: Chemical shift anisotropy tensors of carbonyl, nitrogen, and amide proton nuclei in proteins through cross-correlated relaxation in NMR spectroscopy, *J Am Chem Soc*, 127, 6062-6068, 2005.
Mandel, A. M., Akke, M., and Palmer, A. G., 3rd: Backbone dynamics of Escherichia coli ribonuclease HI: correlations with structure and function in an active enzyme, *J. Mol. Biol.*, 246, 144-163, 1995.
- 525 Massi, F., Johnson, E., Wang, C., Rance, M., and Palmer, A. G., 3rd: NMR R1 rho rotating-frame relaxation with weak radio frequency fields, *J Am Chem Soc*, 126, 2247-2256, 2004.
Nicholson, L. K., Kay, L. E., Baldissari, D. M., Arango, J., Young, P. E., Bax, A., and Torchia, D. A.: Dynamics of methyl groups in proteins as studied by proton-detected ¹³C NMR spectroscopy. Application to the leucine residues of staphylococcal nuclease, *Biochemistry*, 31, 5253-5263, 1992.
- 530 Peng, J. W., and Wagner, G.: Mapping of Spectral Density-Functions Using Heteronuclear Nmr Relaxation Measurements, *J. Magn. Reson.*, 98, 308-332, 1992.
Sareth, S., Li, H., Yamada, H., Woodward, C. K., and Akasaka, K.: Rapid internal dynamics of BPTI is insensitive to pressure. (¹⁵N spin relaxation at 2 kbar, *FEBS letters*, 470, 11-14, 10.1016/s0014-5793(00)01283-7, 2000.
- 535 Sarma, A. V., Anbanandam, A., Kelm, A., Mehra-Chaudhary, R., Wei, Y., Qin, P., Lee, Y., Berjanskii, M. V., Mick, J. A., Beamer, L. J., and Van Doren, S. R.: Solution NMR of a 463-residue phosphohexomutase: domain 4 mobility, substates, and phosphoryl transfer defect, *Biochemistry*, 51, 807-819, 10.1021/bi201609n, 2012.
Schmidt, J. M., Zhou, S., Rowe, M. L., Howard, M. J., Williamson, R. A., and Löhr, F.: One-bond and two-bond J couplings help annotate protein secondary-structure motifs: J-coupling indexing applied to human endoplasmic reticulum protein ERp18, *Proteins*, 79, 428-443, 10.1002/prot.22893, 2011.
- 540 Segawa, T. F., and Bodenhausen, G.: Determination of transverse relaxation rates in systems with scalar-coupled spins: The role of antiphase coherences, *J Magnetic Resonance*, 237, 139-146, 2013.
Slichter, J. P.: *Principles of Magnetic Resonance, Solid-State Sciences*, Springer, Berlin, 1992.
Song, X. J., Yuan, Y., Simplaceanu, V., Sahu, S. C., Ho, N. T., and Ho, C.: A comparative NMR study of the polypeptide backbone dynamics of hemoglobin in the deoxy and carbonmonoxy forms, *Biochemistry*, 46, 6795-6803, 10.1021/bi602654u, 2007.
- 545 Szyperki, T., Luginbuhl, P., Otting, G., Güntert, P., and Wüthrich, K.: Protein dynamics studied by rotating frame ¹⁵N spin relaxation times, *J. Biomol. NMR*, 3, 151-164, 1993.
Wang, T., Weaver, D. S., Cai, S., and Zuiderweg, E. R.: Quantifying Lipari-Szabo model-free parameters from ¹³CO NMR relaxation experiments, *J Biomol NMR*, 36, 79-102, 2006.
- 550 Weast, R.: *Handbook of Chemistry and Physics 54 ed.*, edited by: Weast, R., CRC Press, 1973.
Williams, C. J., Headd, J. J., Moriarty, N. A.-O., Prisant, M. G., Videau, L. L., Deis, L. N., Verma, V., Keedy, D. A., Hintze, B. J., Chen, V. B., Jain, S., Lewis, S. M., Arendall, W. B., 3rd, Snoeyink, J., Adams, P. D., Lovell, S. C., Richardson, J. S., and Richardson, D. C.: MolProbity: More and better reference data for improved all-atom structure validation, 2018.
- 555 Woessner, D. E.: Nuclear Spin Relaxation in Ellipsoids Undergoing Rotational Brownian Motion, *J. Chem. Phys.*, 37, 647-654, 1962.
Wüthrich, K.: *NMR of Proteins and Nucleic Acids*, John Wiley & Sons, New York, 1986.
Yang, D., and Kay, L. E.: Contributions to conformational entropy arising from bond vector fluctuations measured from NMR-derived order parameters: application to protein folding, *J. Mol. Biol.*, 263, 369-382, 1996.

560

565



11. Appendix.

Computer programs based on Eqs. 3 (R_2) and 6 (R_1).

The program requests a PDB file for which protons are available. The program makes an internal copy of the pdb file. It requests the radius of the sphere of protons to consider, the rotational correlation time, and the spectrometer. The code consists of two loops; the outer loop advances over the amide protons one by one. The inner loop scans the copy of the coordinates and finds all protons (including HN) around the HN at hand for the radius defined. It co-adds all R_2 rates according to Equation 3 and 12.

The program calculating the $^1\text{HA } R_1$ and $^1\text{HN } R_1$ rates are almost identical to the R_2 program, with changed equations. The linear combinations of $R_2(\text{HN})$ and $R_1(\text{HA})$, as governed by Equation 6, was carried out in a spreadsheet, taking into account different amounts of in-phase / anti-phase admixtures based on the integration of model computations with different scalar couplings and acquisition times.

All programs are written in Fortran90, and contain no references to outside libraries. The source codes are available from the author and will be deposited at <https://github.com>.

Computer program based on Eqs. 12 and 13 (below).

Proton-proton cross-correlated R_2 relaxation between just two dipolar vectors ij and ik is, adapted from (Goldman, 1984) and (Fischer et al., 1998)

$$R_{2CC}^{ij-ik} = \frac{1}{10} \left(\frac{\mu_0 \gamma_i \gamma_j \hbar}{4\pi r_{ij}^3} \right) \times \left(\frac{\mu_0 \gamma_i \gamma_k \hbar}{4\pi r_{ik}^3} \right) \times P_2(\cos \theta_{ij-ik}) \left\{ 5\tau_c + \frac{9\tau_c}{1 + \omega_H^2 \tau_c^2} \right\} \quad [13]$$

where θ_{ij-ik} is the angle between the two vectors ij and ik .

The total R_2 relaxation for proton i is then given by

$$R_2^{i-total} = R_2^{ij} + R_2^{ik} \pm R_{2CC}^{ij-ik} \quad [14]$$

However, these individual line widths can only be observed if the transitions for the H_i multiplet are resolved by J-coupling (and/or residual static dipolar coupling). For amide protons, this will not be the case, and one expects an inhomogeneous line consisting of the superposition of many narrow and broader Lorentzian lines corresponding to a multi-spin expansion of Eq [14].



To my knowledge, there is no closed equation describing R_2 cross-correlated relaxation for more than two dipolar vectors.
595 To arrive at an estimation for the effects in a multi- proton spin system, we start from a “solid state NMR” point of view. We
calculate $B_{loc(i)}^\Omega$, the net local magnetic field at center proton i due to the surrounding protons j (Slichter, 1992) in certain
orientation of the magnetic field with respect of the molecule:

$$B_{loc(i)}^\Omega = \frac{\mu_0 \hbar}{4\pi} \sum_{j \neq i}^{j=M} \Phi_{\pm} \left(\frac{\gamma_i \gamma_j}{r_{ij}^3} \right) P_2(\cos \theta_{ij}) \quad [15]$$

Here, θ_{ij} is the angle between the internuclear vector ij and the magnetic field direction Ω in the molecular frame. Φ_{\pm}
600 represents a certain configuration of the signs of the surrounding dipoles j . For instance, for 10 protons one has 1024 different
configurations. If one varies the magnetic field direction according to a sphere distributions and adds the results one obtains
the cross-correlated powder pattern for that value of Φ_{\pm} . Subsequently one co-adds all powder patterns for different values
of Φ_{\pm} , and normalizes, to arrive at the “cross correlated” dipolar powder pattern for the ^1HN under consideration.

It is the time-dependence of B_{loc} as caused by molecular motion that drives the solution NMR dipolar relaxation. The R_2
605 relaxation is then obtained as the second moment of the (cross-correlated) powder pattern (Slichter, 1992):

$$R_2^{solution} = 4\tau_c \sum_{\Omega} \left(\langle B_{loc} \rangle - B_{loc}^\Omega \right)^2 \quad [16]$$

where the brackets indicate average.

610 The computer program requires as input a “protonated” PDB file (HN for amides), the radius of the sphere of protons
around the amide protons, the rotational correlation time and the spectrometer frequency. Basically, the program consists of
four nested loops: amides, protons around amides, permutation of dipole signs of these surrounding protons, and rotation of
the magnetic field vector in the molecular frame.

A set of 10 nested loops permutes the dipolar signs of the closest 10 hydrogens (1024 distributions). The more remote
615 hydrogens in the sphere (if any) have their dipolar signs assigned according to a 50% random chance.

At the inner most level, a closed loop generates an isotropic spherical distribution (5000 orientations) for the (unit) “magnetic
field” vector (<http://corysimon.github.io/articles/uniformdistn-on-sphere/>).

The angle between the (unit) magnetic field vector and the dipolar vector between HN and the surrounding proton
is computed as the arccosine of the (normalized) dot product of those vectors.

620 The local dipolar field of an individual surrounding proton at ^1HN is then calculated according to Equation 14.

This is repeated for all surrounding protons in the shell and co-added.



At this stage the program has the local field for a certain ^1HN , in a certain orientation, for a certain permutation of surrounding dipole signs. This repeated for all 5000 orientations, so that it obtains the ^1HN powder pattern for a certain permutation of the surrounding dipole signs.

625 Subsequently the corresponding solution NMR line width is computed from this distribution by the method of second moments (Equation 15).

The next step is to repeat this for all 1024 permutations. The line widths are all added and normalized yielding the inhomogeneous linewidth. The inverse line widths, which are proportional to the peak height, are also added.

After that the outer loop advances to the next HN.

630 The program is written in Fortran90, and contains no references to outside libraries. The source code is available from the author and will be deposited at <https://github.com>.



Comparison of cross-correlated and non-cross correlated R_2 relaxation.

635 Figure A1 shows a comparison between the line widths computed for GB1 with and without cross correlation. The data with
cross correlations was computed using the “solid state” approach above, taking into account all protons within a sphere of 6
Å. For the non-cross correlated data, we used the same approach, but instead of calculating 1024 different specific
permutations, we used 1024 random distributions of surrounding dipoles, and averaged those. The Figure shows that there can
be upto 1.5 Hz differences between the two methods, but there is no systematic change, and is of no relevance to our current
640 level of computational precision. But if future calculations ask for refinement, one must include the cross correlations.

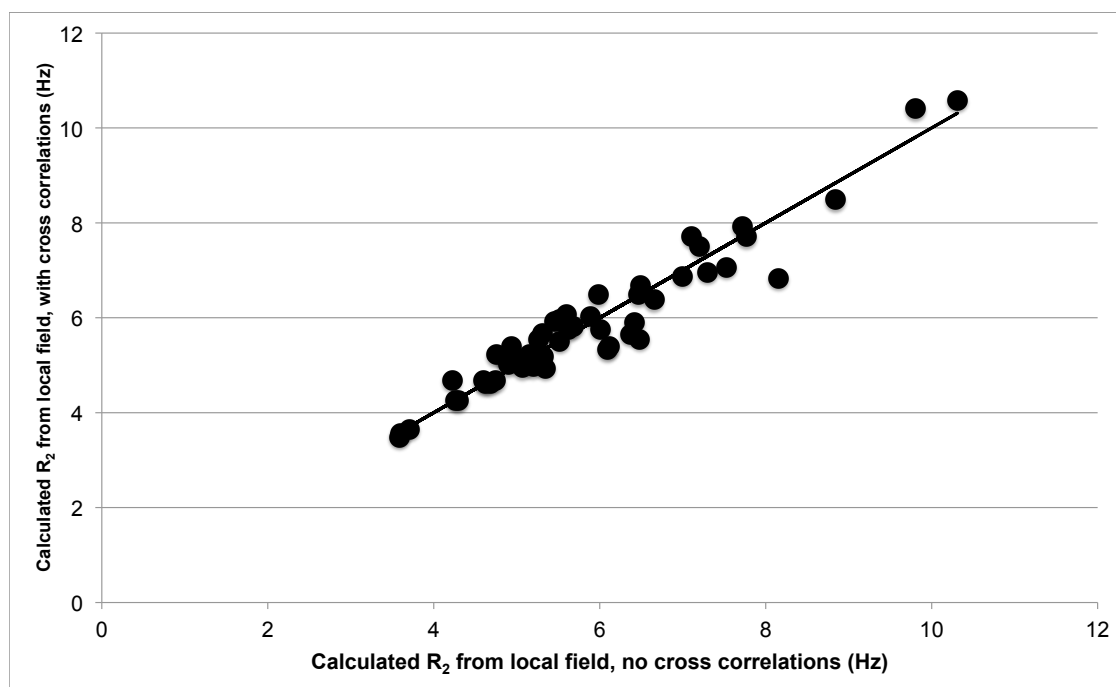


Figure A1.

The effect of R_2 dipolar cross correlations on the ^1HN R_2 for GB1.

2. Rotational correlations times

645

(Daragan and Mayo, 1997) noted a deviation between the τ_c values calculated for proteins from the Stokes-Einstein relation and the experimental values, which were then known for proteins smaller than 18 kDa. Fitting to that data, they obtained the empirical M_r vs. τ_c relationship:

$$650 \quad \tau_c = N_{RES}^{0.93} \frac{9.18 \times 10^{-3}}{T} \exp\left(\frac{2416}{T}\right) \quad (ns). \quad [17]$$

with T in °K. We collected several more experimental rotational correlation times (see Table A1), and find that equation 17 also holds outside the range for which it was developed.

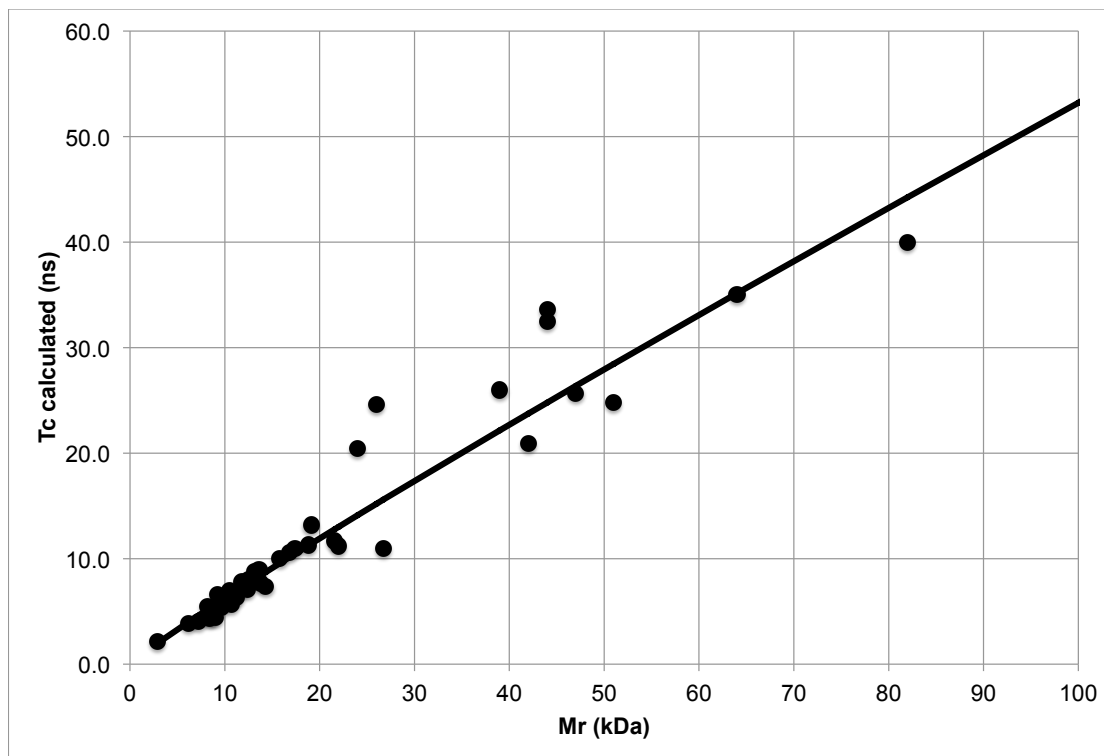


Figure A2. Experimentally determined rotational correlation times for different protein masses (dots) as collected from the literature, measured or corrected to 298K using the known temperature dependency of the water viscosity (see Table A1). The drawn line was computed using Equation 17, also at 298K.



Table A1. Experimental M_r and τ_c data.

Protein	M_r (kDa)	τ_c (ns)	Temperature (°C)	τ_c @ 25 °C in H ₂ O ^a (ns)
Xfin-zinc ^b	2.93	2.4	20	2.1
BPTI ^b	6.16	4.4	20	3.9
B-domain ^c	7.2	4.05	25	4.0
Eglin ^b	8.15	6.2	20	5.5
Calbindin-D9k ^b	8.43	4.9	20	4.3
Calbindin-D9k ^b	8.43	5.1	20	4.55
Ubiquitin ^b	8.54	5.4	20	4.8
Ubiquitin ^c	9.0	4.4	25	4.4
StR82 ^c	9.2	6.6	25	6.6
Cytochrome b5 ^b	9.61	6.1	20	5.4
Barstar ^b	10.14	7.4	20	6.5
TR80 ^c	10.5	7.0	25	7.0
HR2873B ^c	10.7	5.7	25	5.7
DvR115G ^c	10.9	6.5	25	6.5
VfR117 ^c	11.2	6.3	25	6.3
MrR110B ^c	11.8	7.8	25	7.8
BcR147A ^c	11.9	7.2	25	7.2
SyR11 ^c	12.4	7.1	25	7.1
VpR247 ^c	12.5	8.1	25	8.1
BcR97A ^c	13.1	8.8	25	8.8
PfR193A ^c	13.6	9.0	25	9.0
SoR190 ^c	13.8	7.7	25	7.7
Lysozyme ^b	14.32	8.3	20	7.3
ER541-37-162 ^c	15.8	10.0	25	10.0
NsR431C ^c	16.8	10.6	25	10.6
Interleukin-1b ^b	17.4	12.4	20	11.0
ER540 ^c	18.8	11.3	25	11.3
Leuk Inh Fact ^b	19.1	14.9	20	13.2



HIV-1 ^b	21.58	13.2	20	11.7
HIV protease ^d	22	10.7	27	11.2
Trp-repressor ^b	24	23.1	20	20.4
DnaK SBD ^e	26	22.0	30	24.6
Savinase ^b	26.7	12.4	20	11.0
IS- dehydrase ^f	39	18.4	42	26.0
Maltose BP ^g	42	16.2	37	20.9
Hsc70NBD ^h	44	30.0	30	33.6
DnaK NBD ⁱ	44	29.0	30	32.5
CAP ^j	47	22.0	32	25.7
PMM/PGM ^k	51	20.0	35	24.8
Hemoglobin ^l	64	32.0	29	35.0
Malate Synthase ^m	82	37.0	37 in D2O	40

655

Legend to Table A1:

- (a) converted using (Weast, 1973)
- (b) Values listed in (de la Torre et al., 2000)
- 660 (c) Experimental values from the North East Structural Genomics initiative listed at
http://www.nmr2.buffalo.edu/nesg.wiki/NMR_determined_Rotational_correlation_time
- (d) A. Bax, personal communication
- (e) Experimental value from (Bertelsen et al., 2009)
- (f) Experimental value from (Copié et al., 1996)
- 665 (g) Experimental value from (Gardner et al., 1998)
- (h) Experimental value from Weaver, D., Ph.D. thesis, University of Michigan, 2010
<http://hdl.handle.net/2027.42/75930>
- (i) Experimental value from (Korzhnev et al., 2004)
- (j) C. Kalodimos, personal communication
- 670 (k) Experimental value from (Sarma et al., 2012)
- (l) Experimental value from (Song et al., 2007)
- (m) L. Kay and V. Tugarinov, personal communication.